applied sciences

MDPI

Article

Biomechanical Evaluation of Biodegradable Implants Using Anchoring Fixation Sutures in Apical Prolapse Repair

Ana Telma Silva [1,2], Nuno Miguel Ferreira [1,2], Maria Francisca Vaz [1], Marco Parente [1,2], António Augusto Fernandes [1,2] and Maria Elisabete Silva [1,2,*]

[1] LAETA, INEGI, Campus da FEUP Rua Dr. Roberto Frias 400, 4200-465 Porto, Portugal; tcsilva@inegi.up.pt (A.T.S.); nmferreira@inegi.up.pt (N.M.F.); fvaz@inegi.up.pt (M.F.V.); mparente@fe.up.pt (M.P.); aaf@fe.up.pt (A.A.F.)
[2] Faculty of Engineering, University of Porto, Rua Dr. Roberto Frias s/n, 4200-465 Porto, Portugal
* Correspondence: mesilva@fe.up.pt

Abstract

Apical prolapse, a common form of Pelvic Organ Prolapse (POP), is often linked to weakened support structures such as the uterosacral (USL) and cardinal ligaments (CL), influenced by factors like vaginal childbirth, aging, and obesity. Although surgical mesh use is expected to increase, the Food and Drug Administration (FDA) banned polypropylene mesh for transvaginal anterior compartment prolapse in 2019 due to safety concerns, highlighting the need for alternatives such as biodegradable implants. This study developed four biodegradable mesh implants (square and sinusoidal geometries) mimicking the USL and CL. These were applied within a computational pelvic model to assess biomechanical behavior during the Valsalva maneuver and to explore different fixation methods (continuous, interrupted and simple stitch sutures). Baseline analysis of the healthy model established vaginal displacement under normal conditions. Without implant support, complete CL rupture increased displacement by 34%, and complete USL rupture raised displacement by 69%. Polycaprolactone implants consistently reduced anterior vaginal wall displacement in all impairment scenarios. Square implants mimicking the USL reduced displacement by up to 10% in cases of complete USL rupture with intact CL. Similarly, square implants mimicking the CL reduced displacement by up to 15% with complete CL rupture and healthy USL. Simulations with both ligaments impaired showed that USL contribute to support, while CL play a key role in stabilization. These findings demonstrate the potential of biodegradable implants to enhance POP repair. However, further studies are needed to evaluate long-term degradation and clinical applicability.

Keywords: pelvic organ prolapse; biodegradable PCL meshes; finite element analysis

Check for updates

Academic Editor: Paolo Renna

Received: 16 March 2026
Revised: 15 April 2026
Accepted: 18 April 2026
Published: 22 April 2026

Copyright: © 2026 by the authors. Licensee MDPI, Basel, Switzerland. This article is an open access article distributed under the terms and conditions of the Creative Commons Attribution (CC BY) license.

1. Introduction

Pelvic organ prolapse (POP) is a prevalent condition that significantly impacts the quality of life for women. It occurs when one or more pelvic organs protrude through the vagina, outside the pelvis. Research indicates that up to 50% of women may experience POP at some point in their lives [1,2]. The risk factors include vaginal childbirth, advancing age, obesity, menopause, or increased intra-abdominal pressure (IAP) [3,4].

Apical prolapse, particularly affecting the uterus or vaginal vault, is a common form of POP often associated with weakened support structures at the apex, such as the uterosacral ligaments (USL) and cardinal ligaments (CL) [5]. The CL and USL are pelvic ligaments

that connect organs to the body wall, containing vessels, nerves, connective tissue, and adipose tissue. These ligaments provide structural support, helping maintain the position of distensible organs such as the bladder, vagina, rectum, and uterus [6].

Treatment options for symptomatic POP depend on its severity, ranging from conservative approaches—such as pelvic floor exercises, lifestyle modifications, and vaginal pessaries—for milder cases, to surgical intervention for more advanced stages [7].

Surgical techniques can be classified by approach (vaginal or abdominal) and by the repair material used (native tissue or synthetic meshes). Native tissue repair carries significant risks of anatomical and functional recurrence, with reported rates ranging from 16% to 29%, particularly in cases of advanced prolapse or poor tissue quality [8].

To address these limitations, synthetic meshes were introduced as an alternative. Devices such as the Restorelle® Direct Fix—a lightweight polypropylene mesh for transvaginal anterior compartment repair—initially showed promise in terms of surgical handling and short-term outcomes [9]. However, long-term follow-up studies revealed high rates of mesh-related complications (MRCs), including exposure, erosion, chronic pelvic pain, and dyspareunia, significantly affecting patient quality of life [10]. In response, the U.S. Food and Drug Administration (FDA) classified transvaginal meshes as high-risk devices in 2016 and banned their sale for anterior POP repair in 2019 [11,12].

This scenario highlights the critical need for safer and more effective alternatives. Reoperation rates following mesh surgery remain high—up to 30%—and experts project a 47% increase in POP surgical demand over the next 40 years due to demographic trends [13,14]. In addition, mesh anchoring failure has been reported in 38% of patients, occurring on average 1.8 years after implantation [15].

These challenges have driven growing interest in biodegradable mesh implants, which aim to combine the structural support of synthetic meshes with a safer degradation profile. The ideal implant should offer flexibility for surgical handling, mechanical strength for organ support, and a porous architecture ($\geq$75 μm) to promote fibroblast infiltration, tissue integration, and reduce the risk of immune rejection and erosion [13,16].

Recent advances in 3D printing and biomaterials have focused on poly(ϵ-caprolactone) (PCL), an FDA-approved, biocompatible, and slowly biodegradable polyester. PCL degrades over 2–3 years and has shown promise in early studies for reducing MRCs while maintaining mechanical performance [17,18].

Building on these developments, several studies have advanced the use of biodegradable PCL-based meshes for pelvic floor repair. Recent work demonstrated that 3D-printed sinusoidal mesh geometries exhibit distinct stiffness and deformation profiles compared to conventional patterns, highlighting the influence of geometry on the overall mechanical response [19]. The degradation of melt electrowritten PCL scaffolds has been characterized, confirming adequate long-term mechanical stability during tissue regeneration [20]. Medical-grade PCL has also been validated for reproducible mesh fabrication with consistent mechanical performance [21]. In parallel, auxetic designs have been explored to improve flexibility and conformability under physiological loading [22], and antibiotic-coated meshes have been proposed to reduce postoperative infection risks [23].

Simultaneously, significant efforts have been dedicated to computational modelling to investigate the behavior of different mesh types, focusing on the displacement and deformation of pelvic structures during pelvic maneuvers, as well as the performance of synthetic mesh implants to replace impaired USL [24,25]. Numerical simulations have also been used to evaluated the effectiveness of different anchoring techniques in sacrocolpopexy surgeries [26].

The objective of this study was to simulate apical prolapse repair surgery by testing two biodegradable mesh geometries—square and sinusoidal—designed to replicate the mechanical behavior of the USL and CL. To this end, these geometries were integrated into a computational model of the pelvic cavity to simulate sacrocolpopexy, using three different suturing techniques: continuous suture, simple stitch, and interrupted suture. The superior-inferior displacement of the anterior vaginal wall was then assessed during the valsalva maneuver across three levels of USL and CL impairment: 50%, 90%, and 100% (total rupture).

2. Materials and Methods

2.1. Computational Model of the Pelvic Cavity

The model was developed by Brandão et al. [27] based on data from a 24-year-old nulliparous woman. It includes several important anatomical structures such as the bladder, uterus, rectum, levator ani (LA) muscles, pelvic fascia, *arcus tendineous fasciae pelvis* (ATFP), USL, and CL, as shown in Figure 1. The Research Ethics Committee at Centro Hospitalar de São João-EPE, Porto, Portugal (protocol: IRB138/19) granted full approval for this study. This 3D model was validated when it was used to simulate sacrocolpopexy with synthetic implants [26] and to estimate the *in vivo* biomechanical properties of the continent and incontinent woman bladder [28].

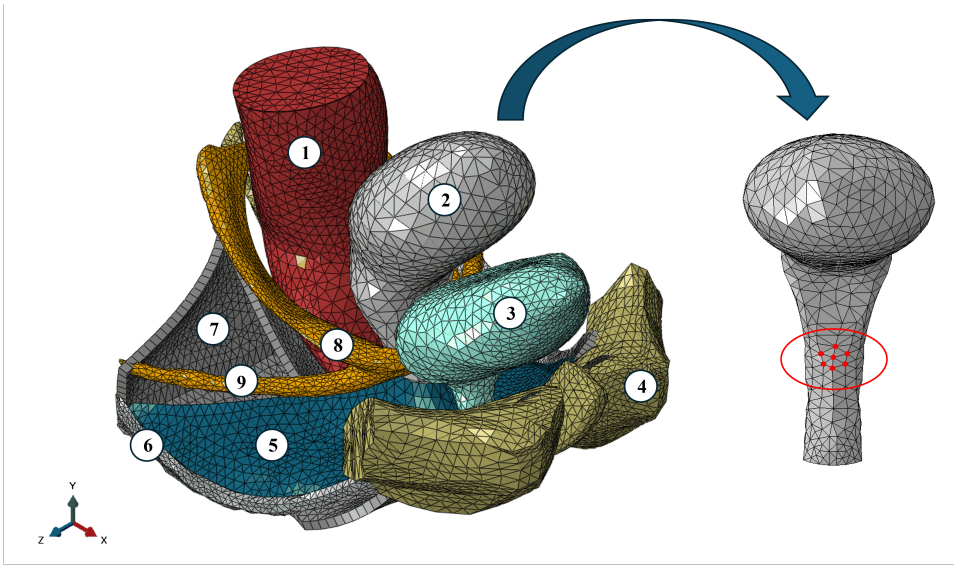

Figure 1. 3D Computational model of the pelvic cavity of an asymptomatic woman. (1) rectum; (2) uterus; (3) bladder; (4) symphysis pubis; (5) pelvic fascia; (6) ATFP; (7) LA muscles; (8) USL; (9) CL. Red dots on the anterior vaginal wall (right) indicate points used to measure supero-inferior displacement.

The Valsalva maneuver—involving forceful exhalation against a closed airway to elevate IAP—is commonly used in urogynecology to evaluate stress urinary incontinence, POP, sphincter integrity, and organ displacement. In this study, the maneuver was passively simulated by applying an IAP of 4 kPa to the LA muscles, pelvic fascia, and the superior surfaces of the bladder and uterus, reflecting typical conditions in young women in the supine position. Fluid interactions within the bladder, uterus, and rectum were simulated using Abaqus® software v.2022 (Dassault Systèmes Simulia Corp., Providence, RI, USA), assuming a density of 1.0×10^{-9} ton/mm^3 [24,29]. Measurements of the anterior vaginal wall were performed at the red nodes shown in Figure 1.

2.2. Biodegradable Implants for the Apical Ligaments

In this study, biodegradable porous implants mimicking the USL and CL were developed (Figure 2) and incorporated into a previously established computational model of the pelvic cavity. The implants were fabricated using PURASORB® PC 12, a medical-grade PCL polymer in pellet form that is commercially available from Corbion [30].

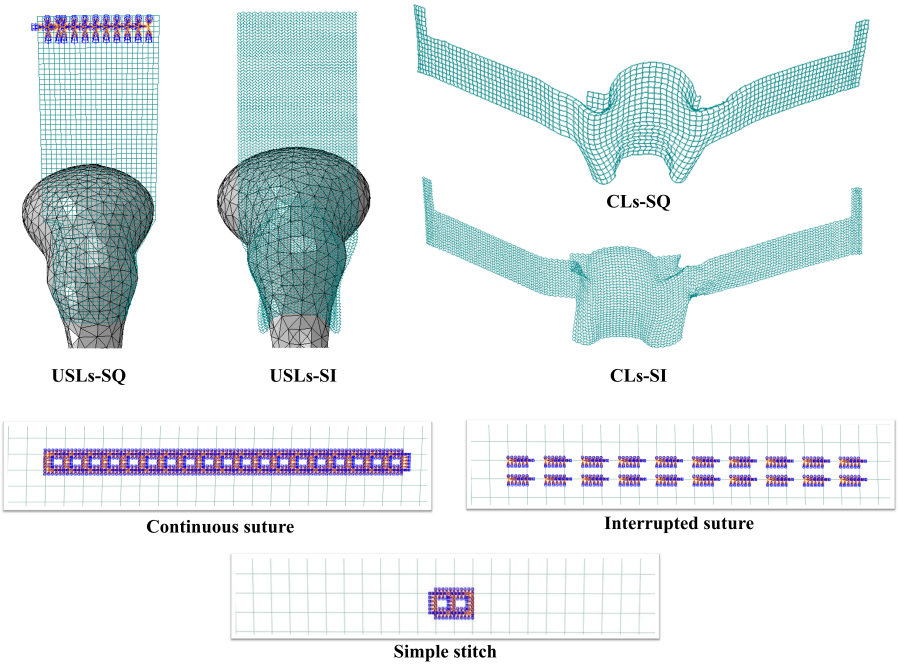

Figure 2. The four computational models of implants used in this study simulate the functionality of the USL and CL: square strip mimicking the USL (USL-SQ), sinusoidal strip mimicking the USL (USL-SI), square strip mimicking the CL (CL-SQ), and sinusoidal strip mimicking the CL (CL-SI), along with the representation of three suture techniques: continuous suture, interrupted suture, and simple stitch.

To simulate anchoring strategies commonly used in surgical procedures, three distinct techniques were included: continuous suture, interrupted suture, and simple stitch. These were integrated into the computational model along with the implants (Figure 2) [26].

The main objective was to evaluate the performance of the biodegradable implants during the valsalva manuever, particularly their capacity to restore support function after partial or complete rupture of the USL and CL.

Using Abaqus® software, 3D meshes with square and sinusoidal geometries, designed to be deformable, were created. To ensure clarity, the primary geometric and computational characteristics of the developed mesh implants are detailed below:

- **Filament Diameter:** A consistent diameter of 240 µm was used for all mesh configurations, determined from previous experimental tests [31].
- **Square Meshes (USL-SQ and CL-SQ):** The geometry for USL-SQ is based on the *DynaMesh-PR* [32], while CL-SQ is based on the *DynaMesh-PRP* [33]. Both feature a pore size of 1.50 mm.
- **Sinusoidal Meshes (USL-SI and CL-SI):** These were developed based on previous studies showing that an auxetic sinusoidal configuration provides dimensionally stable pores under tensile loading, addressing a limitation of current synthetic meshes [19,22]. Due to the complexity of the sinusoidal waves, a slightly larger pore size of 1.58 mm was considered.

- **Overall Dimensions:** The USL-targeting meshes (USL-SQ and USL-SI) have dimensions of 110 × 40 mm. The CL-targeting meshes (CL-SQ and CL-SI), which possess irregular shapes to match the anatomy, have maximum dimensions of 178 × 35 mm.
- **Finite Element Discretization:** All mesh implants were created using B31 beam elements. The mesh densities for each configuration are as follows: USL-SQ: 28,392 nodes and 29,840 elements; USL-SI: 85,241 nodes and 89,640 elements; CL-SQ: 25,177 nodes and 26,430 elements; CL-SI: 67,775 nodes and 71,335 elements.

2.3. Mechanical Properties of the Pelvic Tissues and Biodegradable Mesh Implants

The material properties of biodegradable implants were defined in Abaqus®, assuming a Young's modulus of 251.56 MPa (determined from uniaxial tensile tests on 240 µm printed filaments of medical-grade PCL, as shown in Figure 3) and a Poisson's ratio of 0.3 [31].

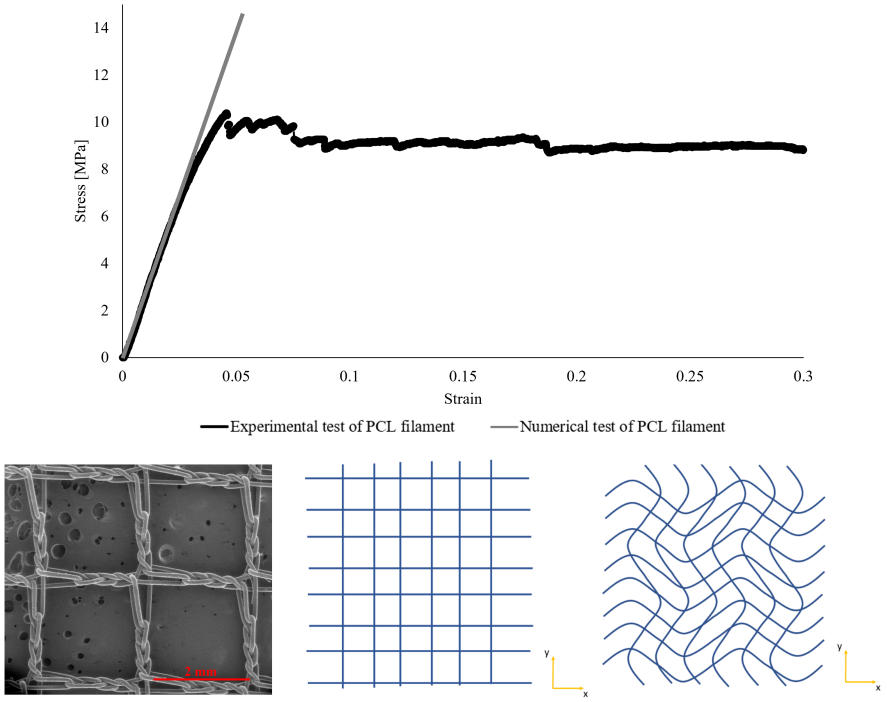

Figure 3. Stress–strain response of medical-grade PCL filaments (240 µm) under uniaxial tensile testing and the numerical curve obtained to determine the modulus of elasticity. (Bottom, from left to right) SEM image of Restorelle® mesh, square mesh geometry and sinusoidal mesh geometry.

Hyperelastic materials, like pelvic floor tissues, exhibit large elastic deformations and a non-linear stress–strain relationship, with stress rising sharply at high strains until failure, which can affect their function [34,35]. To represent this complex mechanical behavior, constitutive models such as Yeoh and Ogden are commonly used. These models assume incompressibility (with the constraint J = 1), which reflects the near-isochoric nature of soft biological tissues under large deformations [36]. Although they do not account for time-dependent effects like viscosity or temperature, they offer reliable predictions of tensile behavior [24,37]. Finite element simulations were conducted in Abaqus®, which handles quasi-incompressible materials by applying a volumetric penalty term to the strain energy density function, ensuring stable and accurate modeling of pelvic cavity tissues.

The Yeoh constitutive model is expressed by Equation (1) [36]:

$$U = \sum_{i=1}^{3} C_i(\bar{I}_1 - 3)^i + \sum_{i=1}^{3} \frac{1}{D_i}(J_{el} - 1)^{2i} \quad (1)$$

where U represents the strain energy density function, which is designed to capture the nonlinear behavior of materials under large deformations. The material parameters (C_i) must be determined experimentally for each specific material [38]. The term $\bar{I}_1$ is the principal strain invariant (Equation (2)) of the right Cauchy–Green strain tensor C (Equation (3)).

$$\bar{I}_1 = \mathrm{tr}(\bar{C}) \quad (2)$$

$$\mathbf{C} = \mathbf{F}^T\mathbf{F} \quad (3)$$

where $\mathbf{F}$, the deformation gradient (Equation (4)), describes the transformation from the reference configuration $\mathbf{X} = (X_1, X_2, X_3)$ to the deformed configuration $\mathbf{x} = (x_1, x_2, x_3)$.

$$\mathbf{F} = \frac{\partial \mathbf{x}}{\partial \mathbf{X}} = \begin{bmatrix} \frac{\partial x_1}{\partial X_1} & \frac{\partial x_1}{\partial X_2} & \frac{\partial x_1}{\partial X_3} \\ \frac{\partial x_2}{\partial X_1} & \frac{\partial x_2}{\partial X_2} & \frac{\partial x_2}{\partial X_3} \\ \frac{\partial x_3}{\partial X_1} & \frac{\partial x_3}{\partial X_2} & \frac{\partial x_3}{\partial X_3} \end{bmatrix} \quad (4)$$

The Ogden strain energy function describes the material behavior in terms of the principal stretches and is expressed as (Equation (5)) [36]:

$$U = \sum_{i=1}^{N} \frac{2\mu_i}{\alpha_i^2}\left(\bar{\lambda}_1^{\alpha_i} + \bar{\lambda}_2^{\alpha_i} + \bar{\lambda}_3^{\alpha_i} - 3\right) + \sum_{i=1}^{N} \frac{1}{D_i}(J_{el} - 1)^{2i} \quad (5)$$

with the modified principal stretches λ_i defined as:

$$\bar{\lambda}_i = J^{-\frac{1}{3}}\lambda_i \rightarrow \bar{\lambda}_1\bar{\lambda}_2\bar{\lambda}_3 = 1. \quad (6)$$

Here, λ_1, λ_2, and λ_3 denote the principal stretches, corresponding to the eigenvalues of the right Cauchy–Green deformation tensor. The material constants μ_n and α_n are determined from experimental measurements, enabling accurate computational modeling of pelvic tissue mechanics. The parameter n indicates the order of the model, specifying the number of terms in the summation [36].

The material parameters for the pelvic structures were derived from experimental studies on cadavers without pelvic dysfunction. These parameters, detailed in the table of Figure 4, enable precise modeling of the stress–strain response within the pelvic cavity under various conditions [26,28].

In this study, simulations were performed to mimic various levels of impairment in the USL and CL, including 50%, 90% (representing a 50% and 90% reduction in stiffness compared to the healthy model), and total (100%) impairment corresponding to total rupture. The simulation of ligament impairment represents a simplified mechanical approximation of prolapse, as anatomical deformation of the pelvic organs was not explicitly modeled. Figure 4 presents the numerical parameters of the Yeoh constitutive model for both healthy and impaired ligaments, as well as the stress–strain curves for the healthy ligaments and those with 50% and 90% impairment.

Structures	α_k	μ_k		Model
Bladder and Urethra	$\alpha_1 = 5.14$	$\mu_1 = 0.19$		Ogden (N = 1)
Rectum	$\alpha_1 = 13.24$ $\alpha_2 = 13.24$	$\mu_1 = 4.25$ $\mu_2 = -3.83$		Ogden (N = 2)
Vagina and Uterus	$\alpha_1 = -3.41$ $\alpha_2 = -0.66$ $\alpha_3 = -6.48$	$\mu_1 = -92.24$ $\mu_2 = 39.29$ $\mu_3 = 54.68$		Ogden (N = 3)
Pelvic ligaments (PUL)	$\alpha_1 = 10.95$	$\mu_1 = 1.58$		Ogden (N = 1)
	c_1 [MPa]	c_2 [MPa]	c_3 [MPa]	**Model**
Pubocervical fascia	0.93	−0.62	0.47	Yeoh
ATFP, CL, USL, LLR	1.74	6.60	4.79	Yeoh
PFM	0.003	0.002	0.001	Yeoh

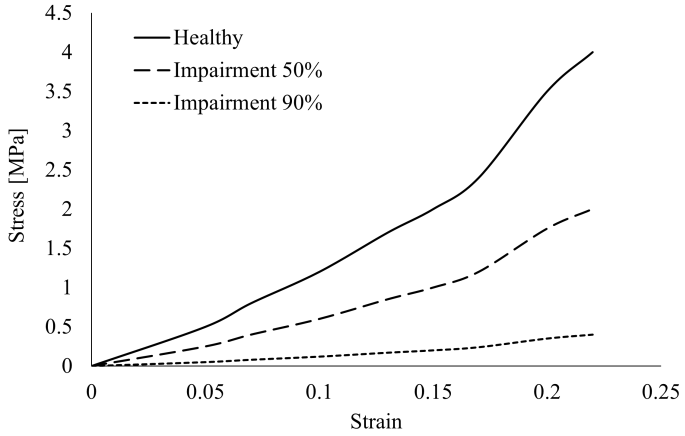

Figure 4. The table (adapted from [26]) shows the material parameters for different pelvic structures. The figure presents stress–strain curves for healthy ligaments and ligaments with 50% and 90% impairment, along with the numerical parameters of the Yeoh constitutive model for both healthy and impaired ligaments.

3. Results

The effectiveness of various implant designs was evaluated by comparing a healthy pelvic model with simulations that incorporated biodegradable implants into the pelvic cavity. Table 1 presents the supero-inferior displacements and their maximum magnitudes, including the values for a healthy model, cases with 50% and 90% impairments, and total ligaments rupture. In addition to studying individual ligament impairments, where one ligament remains intact while the other is impaired at different levels, impairments were applied to both ligaments. Specifically, a 90% impairment was applied to one ligament, while varying impairment levels (50%, 90%, and total rupture) were applied to the other. This approach aimed to investigate the role of each ligament in uterine support. The variation in supero-inferior displacement was calculated using the healthy model as the reference value.

An analysis of ligament impairment reveals that the USL have a more significant impact on supero-inferior displacement of the anterior vaginal wall than the CL. When the USL are intact but the CL experience a complete rupture, the displacement measures 8.58 mm. Conversely, if the CL remain intact while the USL are fully ruptured, the displace-

ment increases considerably to 10.77 mm. This observation highlights the crucial role of the USL in maintaining structural stability and regulating vertical displacement.

Table 1. Supero-inferior displacement of the anterior vaginal wall for varying degrees of USL (50%, 90%, and total rupture) and CL impairment (50%, 90%, and total rupture), considering both healthy and 90% impaired conditions for the opposing ligament.

Variable		Sup-Inf Disp. (mm)	Max. Disp. Mag. (mm)	Variation Sup-Inf/ Healthy * (%)
Healthy	Rest	...	...	...
	Valsalva	6.38	7.77	...
	USL Variation			
CL healthy	Imp. 50%	7.03	8.53	10.19
	Imp. 90%	8.91	10.96	39.66
	Total Rupture	10.77	12.49	68.81
CL with imp. 90%	Imp. 50%	8.54	10.42	33.86
	Imp. 90%	10.23	12.55	60.34
	Total Rupture	11.36	12.78	78.06
	CL Variation			
USL healthy	Imp. 50%	6.74	8.23	5.64
	Imp. 90%	7.40	9.10	15.99
	Total Rupture	8.58	10.33	34.48
USL with imp. 90%	Imp. 50%	9.11	10.68	42.79
	Imp. 90%	10.23	12.55	60.34
	Total Rupture	12.37	15.49	93.89

* Percentage variation in supero-inferior displacement relative to the Healthy Valsalva condition, used as the baseline reference.

Figure 5 presents the supero-inferior displacement measured after the incorporation of different biodegradable implants and the application of varying impairment levels. In this simulation, the anchoring points correspond to a continuous suture, as shown in Figure 2.

The primary objective of this study was to evaluate which implant best mimics the mechanical behavior of healthy ligaments. In particular, the target displacement value of healthy ligaments is 6.38 mm, serving as a reference for comparison. Therefore, regardless of the degree of ligament impairment, the implant should exhibit a displacement value as close as possible to this benchmark, ensuring functional and biomechanical compatibility.

In the top graph of Figure 5, it is evident that in cases of total rupture of the USL, the USL-SQ implant most closely resembles the healthy model. However, in cases of 50% impairment of the USL, the USL-SI implant is the one that most closely resembles the healthy model. In bottom graph of Figure 5, the implants designed to mimic the CL (CL-SQ and CL-SI) can only restore the reference position when the USL are intact, underscoring the crucial role of the USL in maintaining structural integrity. Among these implants, CL-SQ provides the closest approximation to the healthy model. When the USL remain intact and the CL undergo total rupture, the CL-SQ implant exhibits a relative difference of approximately 15% compared to the healthy reference. Furthermore, as the impairment of the structures (USL and CL) increases, restoring the healthy model's position becomes progressively more difficult.

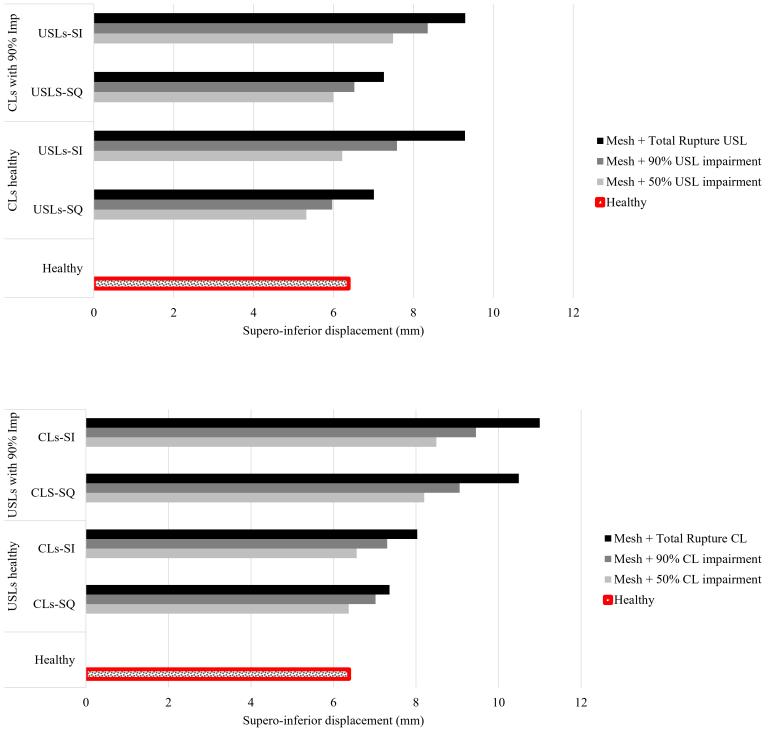

Figure 5. Supero-inferior displacements of the anterior vaginal wall. (**Top**): Cases with varying levels of USL impairment using USL implants, with CL either healthy or 90% impaired; (**Bottom**): Cases with varying levels of CL impairment using CL implants, with USL either healthy or 90% impaired.

Figure 6 presents the superior-inferior displacement obtained from numerical simulations under five conditions: healthy, complete rupture of the CL, incorporation of the CL-SQ implant under 50% impairment of the CL, total rupture of the USL and the incorporation of the USL-SQ implant under 50% impairment of the USL. The results indicate a clear reduction in displacement with implant application, suggesting a trend towards restoring the healthy condition.

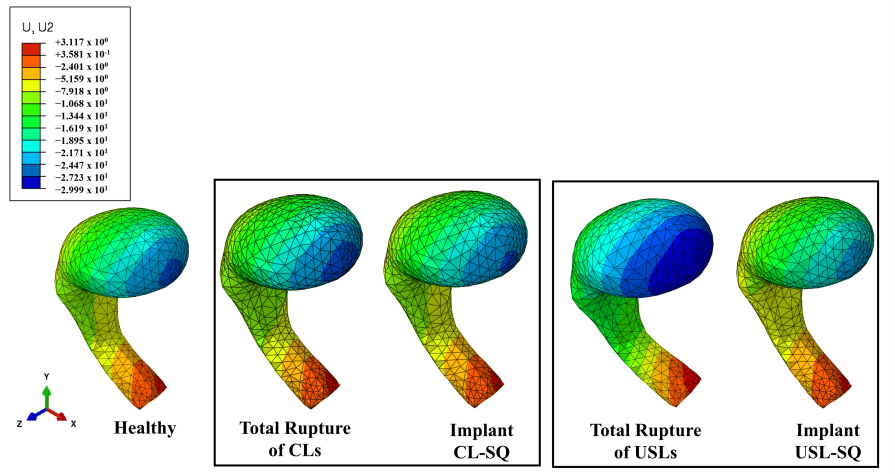

Figure 6. Numerical simulation results of supero-inferior displacement: Healthy; total rupture of the CL and incorporation of the CL-SQ implant under 50% impairment of the CL; total rupture of the USL and the incorporation of the USL-SQ implant under 50% impairment of the USL.

Figure 7 shows the numerical stress–strain curves for the square and sinusoidal meshes developed in this study. For comparison, stress–strain curves of the ligaments and vaginal tissue, obtained from previous studies, are also included [31]. It can be observed that the

sinusoidal mesh exhibits a mechanical response similar to that of vaginal tissue, whereas the square mesh reaches stress levels closer to those of the ligaments [39].

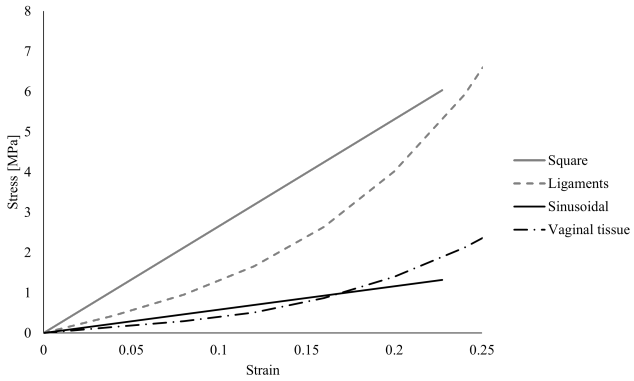

Figure 7. Stress–strain response of square and sinusoidal meshes compared with ligaments and vaginal tissue obtained from fresh female cadavers without POP (adapted from [39]).

Study of Different Fixation Conditions

The study's initial focus was examining different implants' behavior without considering the variation in suturing techniques used by different surgeons. However, an additional analysis, shown in Figure 8, was conducted to investigate the effect of implant fixation on supero-inferior displacement. For this analysis, two anchoring techniques were considered: a simple stitch and an interrupted suture.

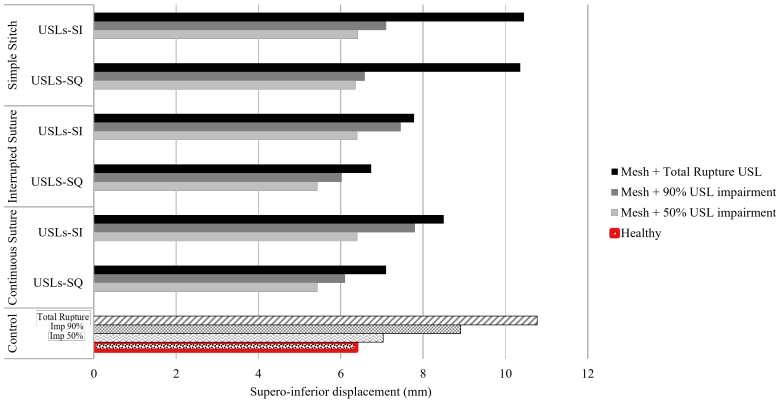

Figure 8. Supero-inferior displacements of the anterior vaginal wall with different fixation methods: interrupted suture, simple stitch, and continuous suture, considering varying levels of USL impairment. Black bars indicate mesh with total USL rupture, dark gray 90% impairment and light gray 50% impairment.

This analysis aimed to evaluate the results from numerical simulations using the developed implants to gain insight into their performance under different fixation approaches, which can vary based on the surgeon's preference. This analysis also aims to understand how the implants behave when mimicking different ligament conditions (impairment of 50%, 90%, and total rupture).

As shown in Figure 8, the USL-SQ implant exhibits lower displacement values than the USL-SI implant across the different fixation methods, both in cases of total rupture and partial ligament impairment. Continuous and simple sutures produce similar displacement values, while the interrupted suture appears to provide better support in cases of total rupture. Notably, with the simple stitch, both implants are unable to recover or provide support under total rupture conditions.

Figure 9 shows that when the implant is fixed with either continuous or interrupted sutures, the USL-SQ implant exhibits a uniform tension distribution across its center. In contrast, high-tension areas are not observed in the USL-SI implant, with the highest values occurring around the uterus. When using a simple stitch, both implants (USL-SQ and USL-SI) display the highest stress concentrations around the embedded elements and in the regions in contact with the uterus.

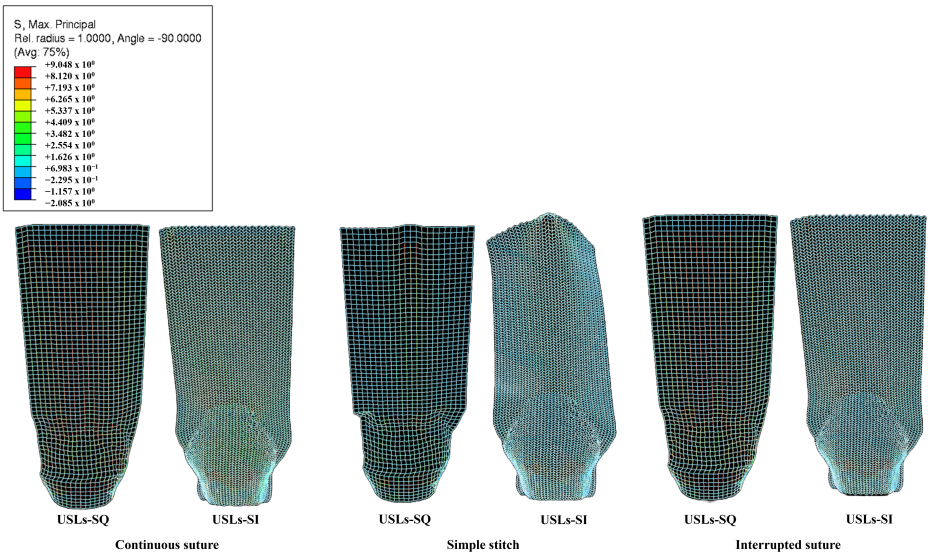

Figure 9. Stress concentration in USL-SQ and USL-SI implants under different fixation methods: continuous suture; simple stitch and interrupted suture.

4. Discussion

This study focused on biodegradable meshes made from medical-grade PCL polymer, designed to mimic the function of USL and CL. The primary objective was to assess the performance of porous biodegradable implants under an IAP of 4 kPa, simulating sacrocolpopexy in a female pelvic cavity model, building on previous research in this field [26].

The supero-inferior displacement of the anterior vaginal wall is directly influenced by the degree of impairment of the USL and CL. When one ligament remains intact while the other is completely ruptured, the displacement increases by 69% in the case of USL rupture and by 34% in the case of CL rupture, compared to the healthy model. This highlights the greater impact of USL impairment on vaginal wall displacement. These findings align with Silva et al. [26], who reported a healthy displacement of 7.69 mm and observed a progressive increase with higher impairment levels.

No studies have explored computational models of biodegradable implants for POP repair. Silva et al. [26] investigated synthetic implants and reported a 27% difference in displacement between a healthy model and cases of total USL rupture. In contrast, the biodegradable USL-SQ implant developed in this study demonstrates superior performance. When assessed in the same region, it reduces the displacement difference to a mere 10%, significantly enhancing its capacity to replicate the biomechanical behavior of natural ligaments. This finding underscores its effectiveness in restoring structural support and minimizing deviations from the healthy model, positioning it as a promising alternative for the treatment of POP.

Restorelle® mesh, despite offering greater stiffness, presents significant drawbacks compared to biodegradable meshes. Its excessive rigidity and twisting behavior further increase stiffness, leading to numerous graft-related complications. Moreover, its non-

biodegradable nature exacerbates these issues, as the mesh remains permanently in the body. In contrast, biodegradable meshes provide sufficient support while gradually degrading, reducing long-term complications. Chen et al. [40] demonstrated that absorbable sutures lower the risk of infections and erosions, highlighting the advantages of biodegradable materials in pelvic repair.

When considering a 90% impairment of the CL with implants that mimic the function of the USL, the resulting increase in displacement is relatively minimal, even as the extent of USL impairment changes. In contrast, applying a 90% impairment to the USL while utilizing implants that mimic the CL leads to a significant increase in displacement, irrespective of the level of CL impairment. These results underscore that the USL play a more critical role in providing structural support compared to the CL, emphasizing their importance in maintaining stability.

These results are in line with biomechanical studies that demonstrated that the USL exhibit higher ultimate tensile strength and a greater tangent modulus in the linear region of the stress–strain curve compared to the CL, indicating a greater load-bearing capacity. Additionally, the USL contain more elastin and dense connective tissue, which contribute to their resilience and ability to recover shape after deformation. The collagen fibers of the USL are oriented along the direction of the load, suggesting that they were evolutionarily designed to withstand significant axial forces, further reinforcing their structural role in uterine support. Structurally, the USL provide direct attachment between the cervix, upper vagina, and the sacrum, forming a strong anchoring system that supports the uterus. In contrast, the CL extend to the upper fascia of the pelvis and primarily support the lateral aspects of the uterus, playing a secondary role in the overall stability of the pelvic organs [41].

In this study, the use of computational models for various implants, designed to mimic the USL and CL, resulted in a reduction of the supero-inferior displacement of the anterior vaginal wall. The biomechanical performance of the biodegradable implants depends on the degree of injury to the USL and CL, as well as the condition of surrounding structures such as muscles and adjacent fascia. The distinct biomechanical behaviors of the square and sinusoidal geometries present important clinical trade-offs. The square configuration, with vertical fibers that resist force from the outset, offers high stiffness. This makes it clinically preferable for severe cases, such as complete ligament rupture, where strong, immediate structural support is required to restore the healthy anatomical position. Conversely, the sinusoidal mesh exhibits an initial stretching phase before reaching maximum resistance and is further characterized by an auxetic response, enabling lateral expansion under tensile loading. This behavior enhances conformability and promotes a more uniform stress distribution. As such, the sinusoidal design is more suitable for partial impairments, as it can dynamically share the mechanical load with the partially functioning native tissue, providing a more physiological mechanical environment, as previous studies by Vaz et al. and Sterk et al. [19,31] demonstrated. However, it must be noted that implants should primarily be compared to the supporting ligaments, which have higher stiffness, rather than just vaginal tissue. As multiple structures become compromised, fully restoring the healthy position becomes progressively more difficult, highlighting the importance of a personalized approach in choosing the implant geometry, tailored to the patient's specific anatomical context.

The interaction between implant geometry and the interdependent mechanical behavior of the USL and CL suggests that spatially heterogeneous designs may offer additional advantages. In particular, hybrid mesh configurations combining square and sinusoidal geometries could enable localized tuning of mechanical properties, with stiffer regions providing structural support at anchoring sites and more compliant, auxetic regions enhancing

conformability and stress distribution in areas interfacing with softer tissues. Although not evaluated in the present study, such designs represent a promising direction for future research and may further improve the biomechanical and clinical performance of biodegradable implants.

In clinical practice, surgeons may employ different fixation and anchoring techniques. In this study, three types of fixation were evaluated: continuous, simple, and interrupted sutures. Once continuous and interrupted sutures were applied, the outcomes obtained were very similar. This finding is noteworthy, as it suggests that comparable fixation can be achieved even with a lower number of suture nodes. In contrast, the results obtained with the simple stitch showed visible differences. Specifically, the supero-inferior displacement values were higher compared to those observed with continuous and interrupted sutures. These findings are consistent with the literature. For example, Silva et al. reported variations of approximately 10% when comparing these two suture techniques under otherwise identical conditions [26].

Traditionally, as highlighted by Pollack et al., the choice of suture for apical prolapse repair has relied more on institutional protocols and surgeon preference than on evidence-based data [42]. However, recent research has increasingly aimed to provide stronger guidance for clinical decision-making. It is now recognized that the type of suture can influence surgical outcomes, particularly in terms of tissue integration with the implant material. According to Raalte et al., accurate and stable fixation is essential for achieving positive surgical results, and various suturing and anchoring devices have been developed over the years to enhance both precision and reliability [43].

When interpreting these findings, it is important to consider the specific characteristics of the chosen model. The pelvic cavity used represents a healthy woman modified to simulate apical prolapse, which may not fully capture the complex anatomy of a typical POP population. Future studies should include more representative cohorts and patient-specific follow-up data to further improve the clinical relevance and validation of the simulations. Furthermore, POP often affects other surrounding structures, such as the pelvic floor muscles [44], which were assumed to be healthy in our simulations. The anatomical representation was also constrained by the absence of the sacrum, and differences in pore orientation and mesh density may impact the comparability of our results. Finally, a significant limitation is the absence of long-term biological follow-up. Although the biodegradable implants were designed to provide temporary mechanical reinforcement, we did not evaluate the biological response—namely post-degradation tissue integration, regeneration, and the effectiveness of load transfer from the implant to native tissue. Addressing existing limitations and pursuing additional research will help improve treatment options and outcomes for women affected by this condition.

5. Conclusions

This study evaluated the biomechanical performance of 3D-printed biodegradable PCL meshes for apical POP repair using a computational modeling approach. The results highlight the critical role of the USL in maintaining apical support, as well as the influence of fixation strategy, with continuous and interrupted sutures providing superior mechanical stability compared to simple stitches.

Importantly, the findings demonstrate that implant geometry significantly affects mechanical behavior. The square configuration provides higher stiffness and immediate load-bearing capacity, making it more suitable for severe prolapse conditions requiring rapid structural support. In contrast, the sinusoidal design, characterized by a more compliant and auxetic response, enables improved conformability and load sharing with surrounding tissues, making it better suited for partial ligament impairment.

Overall, these results support the biomechanical feasibility of biodegradable PCL meshes as a promising alternative to permanent synthetic implants, while emphasizing the importance of tailoring implant design and fixation strategy to patient-specific conditions. Future work should focus on long-term biological validation, including tissue integration and remodeling, as well as the development of optimized, patient-specific implant designs.

Author Contributions: Conceptualization, M.E.S.; methodology, A.T.S. and N.M.F.; software, A.T.S. and M.P.; validation, A.A.F. and M.E.S.; formal analysis, A.T.S. and N.M.F.; investigation, A.T.S.; resources, M.E.S.; data curation, A.T.S. and N.M.F.; writing—original draft preparation, A.T.S.; writing—review and editing, M.F.V. and M.E.S.; visualization, M.F.V. and M.P.; supervision, A.A.F. and M.E.S.; project administration, M.E.S.; funding acquisition, A.A.F. All authors have read and agreed to the published version of the manuscript.

Funding: This research was funded by Fundação para a Ciência e a Tecnologia (FCT) through the financial support to LAETA under project UID/50022/2025 (DOI: https://doi.org/10.54499/UID/50022/2025), the Stimulus of Scientific Employment 2021.00077.CEECIND, and the PhD grants 2024.00925.BD and 2025.05959.BDANA.

Institutional Review Board Statement: The study was conducted in accordance with the Declaration of Helsinki, and approved by the Ethics Committee at Centro Hospitalar de São João-EPE, Porto, Portugal (protocol: IRB138/19).

Informed Consent Statement: Informed consent was obtained from all subjects involved in the study.

Data Availability Statement: The original contributions presented in this study are included in the article. Further inquiries can be directed to the corresponding author.

Acknowledgments: The authors acknowledge FCT for its financial support to LAETA via the project UID/50022/2025 (DOI: https://doi.org/10.54499/UID/50022/2025). This research was also supported by the FCT Stimulus of Scientific Employment (2021.00077.CEECIND) and by the FCT PhD grants 2024.00925.BD and 2025.05959.BDANA.

Conflicts of Interest: The authors declare no conflicts of interest.

Abbreviations

The following abbreviations are used in this manuscript:

ATFP	*Arcus tendineous fasciae pelvis*
CL	Cardinal ligaments
CL-SQ	Square strip mimicking the CL
CL-SI	Sinusoidal strip mimicking the CL
FDA	Food and Drug Administration
IAP	Intra-abdominal pressure
LA	Levator ani
MRCs	Mesh-related complications
PCL	Poly(ϵ-caprolactone)
POP	Pelvic Organ Prolapse
USL	Uterosacral ligaments
USL-SQ	Square strip mimicking the USL
USL-SI	Sinusoidal strip mimicking the USL

References

1. Baah-Dwomoh, A.; Vita, R.D. Effects of repeated biaxial loads on the creep properties of cardinal ligaments. *J. Mech. Behav. Biomed. Mater.* **2017**, *74*, 128–141. [CrossRef]
2. Chung, S.H.; Kim, W.B. Various Approaches and Treatments for Pelvic Organ Prolapse in Women. *J. Menopausal Med.* **2018**, *24*, 155. [CrossRef]

3. Molina, R.A.P.; Martínez, A.H.; Vázquez, S.M.; Galiano, J.M.M. Influence of pelvic floor disorders on quality of life in women. *Front. Public Health* **2023**, *11*, 1180907. [CrossRef]
4. Kuittinen, T.; Mentula, M.; Tulokas, S.; Brummer, T.; Jalkanen, J.; Tomas, E.; Mäkinen, J.; Sjöberg, J.; Härkki, P.; Rahkola-Soisalo, P. Recurrent pelvic organ prolapse after hysterectomy; a 10-year national follow-up study. *Arch. Gynecol. Obstet.* **2024**, *310*, 2705–2715. [CrossRef]
5. Kieserman-Shmokler, C.; Swenson, C.W.; Chen, L.; Desmond, L.M.; Ashton-Miller, J.A.; DeLancey, J.O. From molecular to macro: The key role of the apical ligaments in uterovaginal support. *Am. J. Obstet. Gynecol.* **2020**, *222*, 427–436. [CrossRef]
6. Ramanah, R.; Berger, M.B.; Parratte, B.M.; DeLancey, J.O.L. Anatomy and histology of apical support: A literature review concerning cardinal and uterosacral ligaments. *Int. Urogynecol. J.* **2012**, *23*, 1483–1494. [CrossRef]
7. Mančinskienė, D.; Mikėnaitė, M.; Barakat, M.; Kačerauskienė, J.; Railaitė, D.R.; Maleckienė, L.; Bartusevičius, A.; Bartusevičienė, E. Quality of Life after Treatment for Pelvic Organ Prolapse in Real-World Study: Recommendations, Vaginal Pessary, and Surgery. *Medicina* **2024**, *60*, 547. [CrossRef]
8. Guler, Z.; Roovers, J.P. Role of Fibroblasts and Myofibroblasts on the Pathogenesis and Treatment of Pelvic Organ Prolapse. *Biomolecules* **2022**, *12*, 94. [CrossRef] [PubMed]
9. Goh, Y.M.; Lim, S.H.; Chua, H.L.; Han, H.C.; Lee, J.C. Long-Term Outcomes of Restorelle® Direct Fix Anterior Mesh in the Treatment of Pelvic Organ Prolapse. *Cureus* **2024**, *16*, e63513. [CrossRef] [PubMed]
10. Gauthier, A.; Ferry, P.; Bertherat, P.; Tayrac, R.D.; Fernandez, H. Transvaginal treatment of anterior and apical genital prolapse using Restorelle® direct fix™: An observational study of medium-term complications and outcomes. *J. Gynecol. Obstet. Hum. Reprod.* **2020**, *49*, 101674. [CrossRef] [PubMed]
11. US Food and Drug Administration. FDA Takes Action to Protect Women's Health, Orders Manufacturers of Surgical Mesh Intended for Transvaginal Pelvic Organ Prolapse Repair to Stop Sales and Distribution. 2019. Available online: https://www.prnewswire.com/news-releases/fda-takes-action-to-protect-womens-health-orders-manufacturers-of-surgical-mesh-intended-for-transvaginal-repair-of-pelvic-organ-prolapse-to-stop-selling-all-devices-300833010.html (accessed on 10 January 2025).
12. Degirmenci, Y.; Stewen, K.; Dionysopoulou, A.; Schiestl, L.J.; Hofmann, K.; Skala, C.; Hasenburg, A.; Schwab, R. Trends in Urogynecology—Transvaginal Mesh Surgery in Germany. *J. Clin. Med.* **2024**, *13*, 987. [CrossRef]
13. Dabica, A.; Balint, O.; Olaru, F.; Secosan, C.; Balulescu, L.; Brasoveanu, S.; Pirtea, M.; Popin, D.; Bacila, I.F.; Pirtea, L. Complications of Pelvic Prolapse Surgery Using Mesh: A Systematic Review. *J. Pers. Med.* **2024**, *14*, 622. [CrossRef]
14. Chohan, N.; Tyagi, V. Surgical management of pelvic organ prolapse. *Obstet. Gynaecol. Reprod. Med.* **2024**, *34*, 218–228. [CrossRef]
15. Shek, K.L.; Wong, V.; Lee, J.; Rosamilia, A.; Rane, A.J.; Krause, H.; Goh, J.; Dietz, H.P. Anterior compartment mesh: A descriptive study of mesh anchoring failure. *Ultrasound Obstet. Gynecol.* **2013**, *42*, 699–704. [CrossRef] [PubMed]
16. Dällenbach, P. To mesh or not to mesh: A review of pelvic organ reconstructive surgery. *Int. J. Women's Health* **2015**, *7*, 331. [CrossRef] [PubMed]
17. Wu, J.; Yao, H.; Yu, L.; Li, H.; Zuo, Y.; Liu, W.; Zhang, C.; Fu, C.; Liu, M. A novel 3D printed type II silk fibroin/polycaprolactone mesh for the treatment of pelvic organ prolapse. *Biomater. Sci.* **2023**, *11*, 7203–7215. [CrossRef]
18. Deshpande, M.V.; Girase, A.; King, M.W. Degradation of Poly(ϵ-caprolactone) Resorbable Multifilament Yarn under Physiological Conditions. *Polymers* **2023**, *15*, 3819. [CrossRef]
19. Sterk, S.; Silva, M.E.; Fernandes, A.A.; Huß, A.; Wittek, A. Development of new surgical mesh geometries with different mechanical properties using the design freedom of 3D printing. *J. Appl. Polym. Sci.* **2023**, *140*, e54687. [CrossRef]
20. Rynkevic, R.; Silva, M.E.; Martins, P.; Mascarenhas, T.; Alves, J.L.; Fernandes, A.A. Characterisation of polycaprolactone scaffolds made by melt electrospinning writing for pelvic organ prolapse correction—A pilot study. *Mater. Today Commun.* **2022**, *32*, 104101. [CrossRef]
21. Vaz, M.F.R.; Martins, J.A.P.; Pinheiro, F.; Ferreira, N.M.; Brandão, S.; Alves, J.L.; Fernandes, A.A.; Parente, M.P.L.; Silva, M.E.T. Medical- and Non-Medical-Grade Polycaprolactone Mesh Printing for Prolapse Repair: Establishment of Melt Electrowriting Prototype Parameters. *Appl. Sci.* **2024**, *14*, 9670. [CrossRef]
22. Ferreira, N.M.; Antoniadi, E.; Silva, A.T.; Silva, A.; Parente, M.; Fernandes, A.; Silva, E. Melt Electrowritten Biodegradable Mesh Implants with Auxetic Designs for Pelvic Organ Prolapse Repair. *J. Manuf. Mater. Process.* **2025**, *9*, 111. [CrossRef]
23. Martins, J.P.; de Sousa, A.S.; de Oliveira, S.C.; Fernandes, A.A.; da Silva, E.T. Antibiotic-Coated Melt Electrowritten Polycaprolactone Meshes: Fabrication and In Vitro Antibacterial Evaluation. *Macromol* **2025**, *5*, 33. [CrossRef]
24. Silva, M.E.T.; Bessa, J.N.M.; Rynkevic, R.; Parente, M.P.L.; Mascarenhas, M.T.; Jorge, R.M.N.; Fernandes, A.A. Simulation of vaginal uterosacral ligament suspension damage, mimicking a mesh-augmented apical prolapse repair. *Proc. Inst. Mech. Eng. Part H J. Eng. Med.* **2022**, *236*, 573–582. [CrossRef] [PubMed]
25. Silva, M.; Parente, M.; Brandão, S.; Mascarenhas, T.; Jorge, R.N. Characterization of the passive and active material parameters of the pubovisceralis muscle using an inverse numerical method. *J. Biomech.* **2018**, *71*, 100–110. [CrossRef]

26. Silva, M.E.; Bessa, J.N.; Parente, M.P.; Mascarenhas, T.; Jorge, R.M.N.; Fernandes, A.A. Effect of mesh anchoring technique in uterine prolapse repair surgery: A finite element analysis. *J. Biomech.* **2021**, *127*, 110649. [CrossRef]
27. Brandão, S.; Parente, M.; Roza, T.H.D.; Silva, E.; Ramos, I.M.; Mascarenhas, T.; Jorge, R.M.N. On the Stiffness of the Mesh and Urethral Mobility: A Finite Element Analysis. *J. Biomech. Eng.* **2017**, *139*, 081002. [CrossRef]
28. Silva, M.E.T.; Pinheiro, F.A.T.; Ferreira, N.M.; Brandão, F.S.; Martins, P.A.; Parente, M.P.L.; Mascarenhas, M.T.; Fernandes, A.A.; Jorge, R.M.N. An estimation of the biomechanical properties of the continent and incontinent woman bladder via inverse finite element analysis. *Proc. Inst. Mech. Eng. Part H J. Eng. Med.* **2024**, *238*, 598–607. [CrossRef] [PubMed]
29. Pstras, L.; Thomaseth, K.; Waniewski, J.; Balzani, I.; Bellavere, F. The Valsalva manoeuvre: Physiology and clinical examples. *Acta Physiol.* **2016**, *217*, 103–119. [CrossRef]
30. Corbion. Bioresorbable Polymers. 2024. Available online: https://www.corbion.com/products/biomedical-products/purasorb (accessed on 20 June 2024).
31. Vaz, F.; Silva, M.E.; Parente, M.; Fernandes, A.A. *Development of 3D Computational Models of Biodegradable Meshes*; Lecture Notes in Bioengineering; Springer: Cham, Switzerland, 2023; pp. 17–28. [CrossRef]
32. DynaMesh®. DynaMesh-PR. 2025. Available online: https://en.dyna-mesh.com/dynamesh-pr-gb/ (accessed on 20 June 2024).
33. DynaMesh®. DynaMesh-PRP. 2025. Available online: https://en.dyna-mesh.com/dynamesh-prp-gb/ (accessed on 20 June 2024).
34. Islam, S.; Zhalmuratova, D.; Chung, H.J.; Kim, C.I. A model for hyperelastic materials reinforced with fibers resistance to extension and flexure. *Int. J. Solids Struct.* **2020**, *193–194*, 418–433. [CrossRef]
35. Stansfield, E.; Kumar, K.; Mitteroecker, P.; Grunstra, N.D.S. Biomechanical trade-offs in the pelvic floor constrain the evolution of the human birth canal. *Proc. Natl. Acad. Sci. USA* **2021**, *118*, e2022159118. [CrossRef]
36. Holzapfel, G.A. *Nonlinear Solid Mechanics: A Continuum Approach for Engineering*; Wiley: Chichester, UK, 2000.
37. Rosen, D.P.; Jiang, J. A comparison of hyperelastic constitutive models applicable to shear wave elastography (SWE) data in tissue-mimicking materials. *Phys. Med. Biol.* **2019**, *64*, 055014. [CrossRef]
38. Noakes, K.F.; Pullan, A.J.; Bissett, I.P.; Cheng, L.K. Subject specific finite elasticity simulations of the pelvic floor. *J. Biomech.* **2008**, *41*, 3060–3065. [CrossRef] [PubMed]
39. Brandão, S.; Parente, M.; Mascarenhas, T.; Silva, A.R.G.; Ramos, I.; Jorge, R.N. Biomechanical study on the bladder neck and urethral positions: Simulation of impairment of the pelvic ligaments. *J. Biomech.* **2015**, *48*, 217–223. [CrossRef] [PubMed]
40. Chen, S.; Liu, Y.; Peng, L.; Chen, Y.; Shen, H.; Luo, D. Comparative study of absorbable suture and permanent suture in sacrocolpopexy: A meta-analysis and systematic review. *Int. Urogynecol. J.* **2023**, *34*, 993–1000. [CrossRef] [PubMed]
41. Tan, T.; Davis, F.M.; Gruber, D.D.; Massengill, J.C.; Robertson, J.L.; Vita, R.D. Histo-mechanical properties of the swine cardinal and uterosacral ligaments. *J. Mech. Behav. Biomed. Mater.* **2015**, *42*, 129–137. [CrossRef]
42. Pollack, B.L.; Popiel, P.; Toaff, M.C.; Drugge, E.; Bielawski, A.; Sacks, A.; Bibi, M.; Friedman-Ciment, R.; Lebron, K.; Alishahian, L.; et al. Permanent Compared With Absorbable Suture in Apical Prolapse Surgery: A Systematic Review and Meta-analysis. *Obstet. Gynecol.* **2023**, *141*, 268–283. [CrossRef]
43. Raalte, H.; Bhatia, N.; Mangel, J.; Ryckebusch, H.; Roovers, J.P. A novel anchoring system for pelvic organ prolapse repair: An observational study. *Int. Urogynecol. J.* **2023**, *34*, 1593–1598. [CrossRef]
44. Conway, C.K.; White, S.E.; Russell, R.; Sentilles, C.; Clark-Patterson, G.L.; Miller, K.S.; Desrosiers, L.; Knoepp, L.R. Pelvic Organ Prolapse: A Review of In Vitro Testing of Pelvic Support Mechanisms. *Ochsner J.* **2020**, *20*, 410–418. [CrossRef]

Disclaimer/Publisher's Note: The statements, opinions and data contained in all publications are solely those of the individual author(s) and contributor(s) and not of MDPI and/or the editor(s). MDPI and/or the editor(s) disclaim responsibility for any injury to people or property resulting from any ideas, methods, instructions or products referred to in the content.